Silver Nanoplates with Special Shapes: Controlled Synthesis and Their Surface Plasmon Resonance and Surface-Enhanced Raman Scattering Properties

Lehui Lu,[†] Atsuko Kobayashi,[‡] Keiko Tawa,[‡] and Yukihiro Ozaki*[,†]

Department of Chemistry, School of Science and Technology, Kwansei Gakuin University, Sanda, Hyogo 669-1337, Japan, and National Institute of Advanced Industrial Science and Technology (AIST), Ikeda, Osaka 563-8577, Japan

Received July 11, 2006. Revised Manuscript Received August 2, 2006

Shape-controlled synthesis of metal nanostructures has opened many new possibilities to design ideal building blocks for future nanodevices. In this work, new types of monodisperse silver nanoplates with complex shapes, namely, a disklike shape and flowerlike shapes, were controllably synthesized in high yield by reducing $[Ag(NH_3)_2]^+$ with ascorbic acid in the presence of silver seed at room temperature. Unlike previous methods for synthesizing the silver nanoplates in the presence of cetyltrimethylammonium bromide (CTAB) micelles, the use of the precursor $[Ag(NH_3)_2]^+$, other than Ag^+, provides a flexible strategy to control the procession of the reduction reaction in a mild way. These silver nanoplates with shapes of disk and flower were shown to possess surface plasmon resonance (SPR) that directly relates to their geometric shapes. As a result of their high anisotropy in shape, the flowerlike silver nanoplates exhibit excellent surface-enhanced Raman scattering (SERS) enhancement ability relative to spherical silver nanoparticles and the disklike silver nanoplates. We believe that with the efficient synthesis and excellent SERS enhancement ability, these novel flowerlike silver nanoplates may find potential applications for biological sensing and labeling systems.

Introduction

Controlling the shape of metal nanostructures is a promising strategy to tailor their physical and chemical properties for various applications in fields such as biological labeling and imaging,[1] catalysis,[2] information technology,[3] sensing,[4] and surface-enhanced Raman scattering (SERS).[5] For instance, studies in nanoparticle catalysis have shown that the cubic platinum nanostructures bound by {100} facets are desirable for hydrogen gas adsorption, while carbon monoxide molecules prefer to adsorb on the buckyball-like platinum nanostructures bounded by {210} facets.[6] Experimental observations and theoretical calculations also indicate that anisotropic metal nanostructures exhibit shape-dependent optical properties.[7] A typical example is that triangular silver nanoplates show three surface plasmon resonance (SPR) bands corresponding to dipole and quadrupole plasmon resonance, and but only one SPR band is observed for spherical silver nanoparticles.[7a,b] High SERS intensity enhancement is likewise observed for the metal nanostructures with complex shapes.[5,8] Importantly, shape control shows a greater versatility for tuning the properties of the metal nanostrutures than can be achieved otherwise. Despite the importance in theoretical studies and practical applications, the challenge to develop effective approaches for systematic

* To whom correspondence should be addressed. Tel.: +81-79-565-8349. Fax: +81-79-565-9077. E-mail: ozaki@kwansei.ac.jp.

[†] Kwansei Gakuin University.

[‡] National Institute of Advanced Industrial Science and Technology.

(1) (a) Schultz, S.; Smith, D. R.; Mock, J. J.; Schultz, D. A. *Proc. Natl. Acad. Sci. U.S.A.* **2000**, *97*, 996. (b) Nicewarner-Peña, S. R.; Freeman, R. G.; Reiss, B. D.; He, L.; Peña, D. J.; Walton, I. D.; Cromer, R.; Keating C. D.; Natan, M. J. *Science* **2001**, *294*, 137. (c) Cao, Y. C.; Jin, R. C.; Mirkin, C. A. *Science* **2002**, *297*, 1536. (d) Haes, A. J.; Van Duyne, R. P. *J. Am. Chem. Soc.* **2002**, *124*, 10596. (e) Schmid, G. *Nanoparticles from Theory to Application*; Wiley−VCH, Weinheim, Germany, 2003. (f) Rosi, N. L.; Mirkin, C. A. *Chem. Rev.* **2005**, *105*, 1547. (f) Caruso, F. *Colloids and Colloid Assemblies*; Wiley−VCH, Weinheim, Germany, 2003.

(2) (a) Schmid, G. *Chem. Rev.* **1992**, *92*, 1709. (b) Ahmadi, T. S.; Wang, Z. L.; Green, T. C.; Henglein, A.; El-Sayed, M. A. *Science* **1996**, *272*, 1924. (c) Burda, C.; Chen, X. B.; Narayanan, R.; El-Sayed, M. A. *Chem. Rev.* **2005**, *105*, 1025.

(3) (a) Sun, S. H.; Murray, C. B.; Weller, D.; Folks, L.; Moser, A. *Science* **2000**, *287*, 1989. (b) Peyser, L. A.; Vinson, A. E.; Bartko, A. P.; Dickson, R. M. *Science* **2001**, *291*, 103.

(4) (a) Favier, F.; Walter, E. C.; Zach, M. P.; Benter, T.; Penner, R. M. *Science* **2001**, *293*, 2227. (b) Tao, A.; Kim, F.; Hess, C.; Goldberger, J.; He, R. G.; Sun, Y. G.; Xia, Y. N.; Yang, P. D. *Nano Lett.* **2003**, *3*, 1229.

(5) (a) Nie, S. M.; Emory, S. R. *Science* **1997**, *275*, 1102. (b) Dick, L. A.; McFarland, A. D.; Haynes, C. L.; Van Duyne, R. P. *J. Phys. Chem. B* **2002**, *106*, 853. (c) Nikoobakht, B.; El-Sayed, M. A. *J. Phys. Chem. A* **2003**, *107*, 3372. (d) dos Santos, D. S., Jr.; Alvarez-Puebla, R. A.; Oliveira, O. S., Jr.; Aroca, R. F. *J. Mater. Chem.* **2005**, *15*, 3045 (e) Xiong, Y.; McLellan, J. M.; Chen, J.; Yin, Y.; Li, Z. Y.; Xia, Y. *J. Am. Chem. Soc.* **2005**, *127*, 17118. (f) Orendorff, C. J.; Gole, A.; Sau, T. K.; Murphy, C. J. *Anal. Chem.* **2005**, *77*, 3261. (g) Kim, K.; Park, H. K.; Kim, N. H. *Langmuir* **2006**, *22*, 3421.

(6) (a) Falicov, L. M.; Somorjai, G. A. *Proc. Natl. Acad. Sci. U.S.A.* **1985**, *82*, 2207. (b) Shi, A. C.; Masel, R. I. *J. Catal.* **1989**, *120*, 421.

(7) (a) Jin, R. C.; Cao, Y. W.; Mirkin, C. A.; Kelly, K. L.; Schatz, G. C.; Zheng, J. G. *Science* **2001**, *294*, 1901. (b) Jin, R. C.; Cao, Y. W.; Hao. E. C.; Métraux, G. S.; Schatz, G. C.; Mirkin, C. A. *Nature* **2003**, *425*, 487. (c) Kelly, K. L.; Coronado, E.; Zhao, L. L.; Schatz, G. C. *J. Phys. Chem. B* **2003**, *107*, 668. (d) Lee, K. S.; El-Sayed, M. A. *J. Phys. Chem. B* **2005**, *109*, 20331. (e) Liz-Marzán, L. M. *Langmuir* **2006**, *22*, 32.

(8) (a) Kottmann, J. P.; Martin, O. J. F. *Phys. Rev. B* **2001**, *64*, 235402. (b) Lu, L. H.; Randjelovic, I.; Capek, R.; Gaponik, N.; Yang, J. H.; Zhang, H. J.; Eychmüller, A. *Chem. Mater.* **2005**, *17*, 5731. (c) Lu, L. H.; Eychmüller, A.; Kobayashi, A.; Hirano, Y.; Yoshida, K.; Kikkawa, Y.; Tawa, K.; Ozaki, Y. *Langmuir* **2006**, *22*, 2605.

10.1021/cm0615875 CCC: $33.50
Published on Web 09/02/2006

manipulation of the shape of metal nanostructures has been met with only limited success.

Constructing novel nanodevices by bottom-up technologies requires highly tunable building blocks whose properties may be rationally designed. Accordingly, it is critical to seek highly versatile synthesis methods for gaining control over the shape of the metal nanostructures, particularly those with unusual shapes. To date, some metals have been effectively processed into the nanostructures with complex shapes, including cubes,[2b,9] stars,[10] rods,[11] plates,[7a,b,12] wires,[13] and branched multipods.[14] In these cases, the nanoplates attract particularly our attention due to their amazing ability to control optical properties. Although a few strategies have been developed for synthesizing the silver nanoplates with cubic,[2b,9] triangular,[7a,b,] and hexagonal shapes,[12c] there is great interest in designing silver nanoplates with other complex shapes. Exploration of these previously unknown nanoplates with high anisotropy and their unusual optical properties can provide new perspectives into the rational design of novel nanomaterials for applications in new-generation nanodevices, SERS, biodiagnosis, and multicolor labels.[7a] In this article, we report for the first time high-yield, controlled synthesis of the silver nanoplates with shapes of disk and flower in aqueous solutions at room temperature, which can inspire synthesis of similar geometric shapes from other materials. We also investigate their SPR properties and evaluate their performance as SERS substrates. Experimental results clearly show that these silver nanoplates exhibit SPR properties directly relating to their geometric shapes, and the flowerlike silver nanoplates show excellent SERS enhancement ability relative to the disklike silver nanoplates and the spherical silver nanoparticles.

Experimental Section

Materials. Silver nitrate, sodium citrate, L-ascorbic acid, ammonia solution (28−30%), potassium chloride, rhodamine 6G (R6G), and adenine were purchased from Wako Pure Chemical Industries, Ltd. Sodium tetrahydroborate and poly(vinylpyrrolidone) (PVP, $M_w \sim 29\,000$ g/mol) were obtained from Sigma-Aldrich, Inc. All reagents were used as received.

Synthesis of Silver Nanoplates with Disk and Flower Shapes. The silver seed was prepared as follows.[11b] An aqueous solution of silver nitrate (0.25 mM, 100 mL) was rapidly mixed with sodium citrate (30 mM, 1 mL). A 3 mL ice-cooled aqueous solution of sodium tetrahydroborate (10 mM) was then added under vigorous stirring. After 30 s, the stirring was stopped. The resultant silver seeds were used after 2 h. Transmission electron microscopy (TEM) examination showed that the single-crystal silver seeds were spherical and had an average diameter of 4 nm.

For the preparation of the $[Ag(NH_3)_2]^+$ solution, an aqueous solution of silver nitrate was first prepared by dissolving 0.50 g of silver nitrate solid in 25 mL of deionized water. Subsequently, 5.5 mL of an ammonia solution was slowly added to the aqueous solution of silver nitrate under vigorous stirring until a transparent solution was obtained.

Typically, for the synthesis of flowerlike silver nanoplates (sample 1), to a 25 mL of aqueous solution was added 4.5 mL of 0.7 mM PVP, 1.5 mL of 30 mM trisodium citrate, 20 μL of 0.12 M $[Ag(NH_3)_2]^+$, and 100 μL of colloidal Ag solution at room temperature. The pH value of the resulting solution is 8.6. After stirring for 2 min, 900 μL of 100 mM ascorbic acid was injected into the above mixture. Within 1 h, the color of the mixed solution changed from slightly yellow, to reddish (typically during 3 min), and then to blue.

For the synthesis of another type of silver nanoplates with flower shape (sample 2), the amount of the silver seed was increased to 200 μL with other experimental conditions unchanged.

For the synthesis of disklike silver nanoplates (sample 3), the amount of the silver seed and ascorbic acid was adjusted to 300 and 80 μL, respectively, while other experimental conditions were similar to those in the synthesis of sample 1.

All the above products were purified by centrifuging at 4500 rpm (1124*g*) for 8 min and then were stored at 5 °C. The concentrations of the silver nanoplates in all the above samples are same ([Ag] = 0.1 mM).

Characterization. Samples for SERS measurements were prepared by drying 5 μL of the aqueous sol on a glass substrate. Samples for X-ray diffraction (XRD) characterization were prepared on glass substrates in a similar method. A total of 5 μL of 10 nM R6G with 10 mM KCl (or 6 M adenine with 10 mM KCl) was then dropped onto the sample on the glass substrate. After 30 min, the substrate was rinsed with deionized water and dried with a stream of air. In a control experiment, 2 mL of colloidal solution was incubated with 50 nM R6G and 10 mM KCl for 30 min and sealed in a thin glass tube (inner diameter, 1.2 mm) for SERS examination. Raman spectra were collected with a 514.5-nm excitation line of an Ar laser by using a NRS-2100 model Raman spectrometer (JASCO) equipped with a nitrogen-cooled charge-coupled device detector. The laser power at the sample position was typically 1.3 mW. Data acquisition time was 10 s with two accumulations. The samples for TEM examination were prepared by adding 10 μL of aqueous sol onto a carbon-coated copper grid; after 1 min an excess solution was removed by a filter paper, and then the samples were allowed to dry in the air at room temperature. TEM images were obtained on a TECNAI F2OG$_2$ TWIN transmission electron microscope operating at 200 kV. TEM images and analytical data were further processed by using ES Vision 4.0 (Emispec system, Inc). XRD patterns of the samples were recorded on a high-resolution X-ray diffractometer (Rigaku, SLX-2000). Cu Kα radiation (wavelength, 1.5405 Å) was used as an incident X-ray source (50 kV, 300 mA). UV−vis extinction spectra were taken using a UV-3101PC UV−vis−NIR scanning spectrophotometer.

(9) (a) Sun, Y. G.; Xia, Y. N. *Science* **2002**, *298*, 2176. (b) Kim, F.; Connor, S.; Song, H.; Kuykendall, T.; Yang, P. D. *Angew. Chem., Int. Ed.* **2004**, *43*, 3673. (c) Yu, D.; Yam, V. W. *J. Am. Chem. Soc.* **2004**, *126*, 13200. (d) Im, S. H.; Lee, Y. T.; Wiley: B.; Xia, Y. N. *Angew. Chem., Int. Ed.* **2005**, *44*, 2154.

(10) (a) Sau, T. K.; Murphy, C. J. *J. Am. Chem. Soc.* **2004**, *126*, 8648. (b) Yamamoto, M.; Kashiwagi, Y.; Sakata, T.; Mori, H.; Nakamoto, M. *Chem. Mater.* **2005**, *17*, 5391. (c) Nehl, C. L.; Liao, H. W.; Hafner, J. H. *Nano Lett.* **2006**, *6*, 683.

(11) (a) Puntes, V. F.; Krishnan, K. M.; Alivisatos, A. P. *Science* **2001**, *291*, 2115. (b) Jana, N. R.; Gearheart, L.; Murphy, C. J. *Chem. Commun.* **2001**, 617. (c) Kim, F.; Song, J. H.; Yang, P. D. *J. Am. Chem. Soc.* **2002**, *124*, 14316. (d) Pileni, M. P. *Nat. Mater.* **2003**, *2*, 145. (e) Martin, B. R.; Dermody, D. J.; Reiss, B. D.; Fang, M.; Lyon, L. A.; Natan, M. J.; Mallouk, T. M. *Adv. Mater.* **1999**, *11*, 102.

(12) (a) Chen, S. H.; Carroll, D. L. *Nano Lett.* **2002**, *2*, 1003. (b) Hao, E. C.; Kelly, K. L.; Hupp, J. T.; Schatz, G. C. *J. Am. Chem. Soc.* **2002**, *124*, 15182. (c) Maillard, M.; Giorgio, S.; Pileni, M. P. *Adv. Mater.* **2002**, *14*, 1084. (d) Pastoriza-Santos, I.; Liz-Marzán, L. M. *Nano Lett.* **2002**, *2*, 903. (e) Métraux, G. S.; Mirkin, C. A. *Adv. Mater.* **2005**, *17*, 412.

(13) (a) Jana, N. R.; Gearheart, L.; Murphy, C. J. *J. Phys. Chem. B* **2001**, *105*, 4065. (b) Kim, J. U.; Cha, S. H.; Shin, K.; Jho, J. Y.; Lee, J. C. *Adv. Mater.* **2004**, *16*, 459. (c) Wiley, B.; Sun, Y. G.; Mayers, B.; Xia, Y. N. *Chem.−Eur. J.* **2005**, *11*, 454.

(14) Chen, S. H.; Wang, Z. L.; Ballato, J.; Foulger, S. H.; Carroll, D. L. *J. Am. Chem. Soc.* **2003**, *125*, 16187.

Results and Discussion

The essence of our proposed synthesis method is the reduction of a silver salt by ascorbic acid in the presence of citrate ions and PVP through the following reactions:

$$C_6H_8O_6 + 2Ag^+ \rightarrow C_6H_6O_6 + 2Ag + 2H^+ \quad (1)$$

To achieve controlled synthesis of the silver nanostructures with desired shapes, one must carefully control the reduction process of silver salts because highly anisotropic nanostructures only become favorable in a slow reduction process.[5e] For this purpose, we chose $[Ag(NH_3)_2]^+$, other than Ag^+, as a precursor in the present experiment as follows.

$$C_6H_8O_6 + 2Ag(NH_3)_2^+ + 2OH^- \rightarrow C_6H_6O_6 + 2Ag + 4HN_3 + 2H_2O \quad (2)$$

The reduction potential E_0^0 for the Ag^+/Ag (aqueous) systems is $+0.7996$ V, but for the redox pairs $Ag(NH_3)^+/Ag$ (aqueous), the reduction potential E_1^0 is $+0.373$ V. The fact that E_0^0 is greater than E_1^0 reveals that due to the formation of the $Ag(NH_3)^+$ complexes with increasing stability, the oxidation activity for the $Ag(NH_3)^+/Ag$ systems becomes weaker than that for the Ag^+/Ag systems, thus making it possible for the reduction reaction 2 to proceed in a mild way. Furthermore, ascorbic acid is a weak reducing agent. The reduction potential E_2^0 for the $C_6H_6O_6/C_6O_8H_6$ system is $+0.17$ V (pH $=$ 3.4) according to *Lange's Handbook of Chemistry*[15] and is pH-dependent. Our initial attempt of using $NaBH_4$ as a reducing agent was less successful probably because of its strong reducing ability (reduction potential: -1.48 V). In the presence of stabilizing agents such as PVP or cetyltrimethylammonium bromide (CTAB), direct reduction of Ag^+ ions by ascorbic acid cannot occur in the acidic conditions.[11b,16] In the previous studies,[11b,16] a NaOH solution was normally added to adjust the reaction solution to a basic pH value because the reduction ability of ascorbic acid increases under the basic environment. For example, when the pH value of the reaction solution is adjusted from 3.4 to 8.4, the change of the reduction potential for the $C_6H_6O_6/C_6O_8H_6$ systems can be evaluated from the Nernst equation, yielding a reduction potential about 0.3 V lower than the one at pH $=$ 3.4. However, the disadvantage of this method is that the basic conditions can lead to the formation of Ag_2O or AgOH precipitation,[11b,16] which is very undesirable for the growth of the highly anisotropic nanostructures. In our case, the use of the $Ag(NH_3)^+$ solution can well-resolve this problem because the cations $Ag(NH_3)^+$ are stable in the basic environment, and the pH value of the resultant solution can be easily varied by controlling the concentration of ammonia.

Structural Analysis of the Silver Nanoplates. In all the syntheses, the concentrations of the $[Ag(NH_3)_2]^+$, PVP, and sodium citrate are kept constant. The shapes of the products can be controlled by simply changing the concentrations of ascorbic acid and colloidal silver. Therefore, for each synthesis of the silver nanoplates, we will report the amount of silver seed and ascorbic acid added. Figure 1a presents a TEM image of sample 1 synthesized by using 100 μL of colloidal silver and 900 μL of ascorbic acid, clearly indicating that the product possesses a flowerlike shape. Further investigation by scanning electron microscopy (SEM) shows that this flowerlike shape is still well-preserved even after transferring the product onto the glass substrate (Supporting Information, Figure S1a). The plate shape is verified by tilting the TEM sample from 0 to $-60°$ to the beam axis, revealing the three-dimensional structure of the flowerlike silver nanoplates (Supporting Information, Figure S1b). The "petals" can be clearly seen on the edge part of the silver nanoplates (inset). A high-resolution TEM (HRTEM) image of a conjuncting area between two "petals" reveals the well-resolved lattice fringes with a fringe spacing of about 2.50 Å, corresponding to the $3 \times \{422\}$ lattice spacing of a face-centered cubic (fcc) metal silver which can be built by three sets of $3 \times \{422\}$ spacing (Figure 1b).[7a,b,12] The forbidden {422} planes have been also observed in other gold,[17] copper,[11d] and silver[7a−b] nanostructures in the form of thin plates or films. The continuous parallel lattice fringes show that neighboring "petals" assume the same crystallographic orientation. The corresponding fast Fourier transform (FFT) of the HRTEM image indicates two sets of sixfold rotational symmetry spots (Figure 1c), suggesting that the basal plane of the flowerlike silver nanoplates is actually presented by {111} crystal planes. The inner set consisting of the strongest six spots is due to the {220} reflection of fcc silver (boxed spot). The ratio between the distance of the diagonal spots in the outer set and that in inner set is 1.730, which is in good agreement with the ratio between the lattice spacing of the {220} planes and that of the {422} planes (1.732). Furthermore, the angle between the neighboring inner and outer spots is measured to be 30°, well consistent with the interplanar angle between the {220} planes and the {422} planes (see Supporting Information). Therefore, the outer set could be ascribed to the forbidden {422} reflection (circled spot). Interestingly, distinct flowerlike silver nanoplates (sample 2) could be obtained through increasing the amount of colloidal silver to 200 μL with the amount of ascorbic acid unchanged (Figure 2a). Compared with sample 1, the "petals" in sample 2 are obviously smaller. When the amount of colloidal silver was increased to 300 μL and that of ascorbic acid decreased to 80 μL, the monodisperse disklike silver nanoplates with average dimensions of 38 nm (thickness) and 90 nm (length) were produced in high yield (sample 3, Figure 2b). These disklike silver nanoplates look like those synthesized by a polystyrene sphere-templating method.[12b] HRTEM images of sample 2 and sample 3 show clear lattice planes similar to that of sample 1, implying that the basal planes of sample 2 and sample 3 are also the {111} crystal planes (inset in Figure 2a,b).

The XRD patterns of sample 1, sample 2, and sample 3, shown in Figure 3, are nearly identical. Namely, an overwhelmingly intensive diffraction line is observed at $2\theta \sim$

(15) Dean, J. A. *Lange's Handbook of Chemistry*; McGraw-Hill: New York, 1985.
(16) Chen, S. H.; Carroll, D. L. *J. Phys. Chem. B* **2004**, *108*, 5500.
(17) (a) Ah, C. S.; Yun, Y. J.; Park, H. J.; Kim, W. J.; Ha, D. H.; Yun, W. S. *Chem. Mater*. **2005**, *17*, 5558. (b) Kan, C. X.; Zhu, X. G.; Wang. G. H. *J. Phys. Chem. B* **2006**, *110*, 4651.

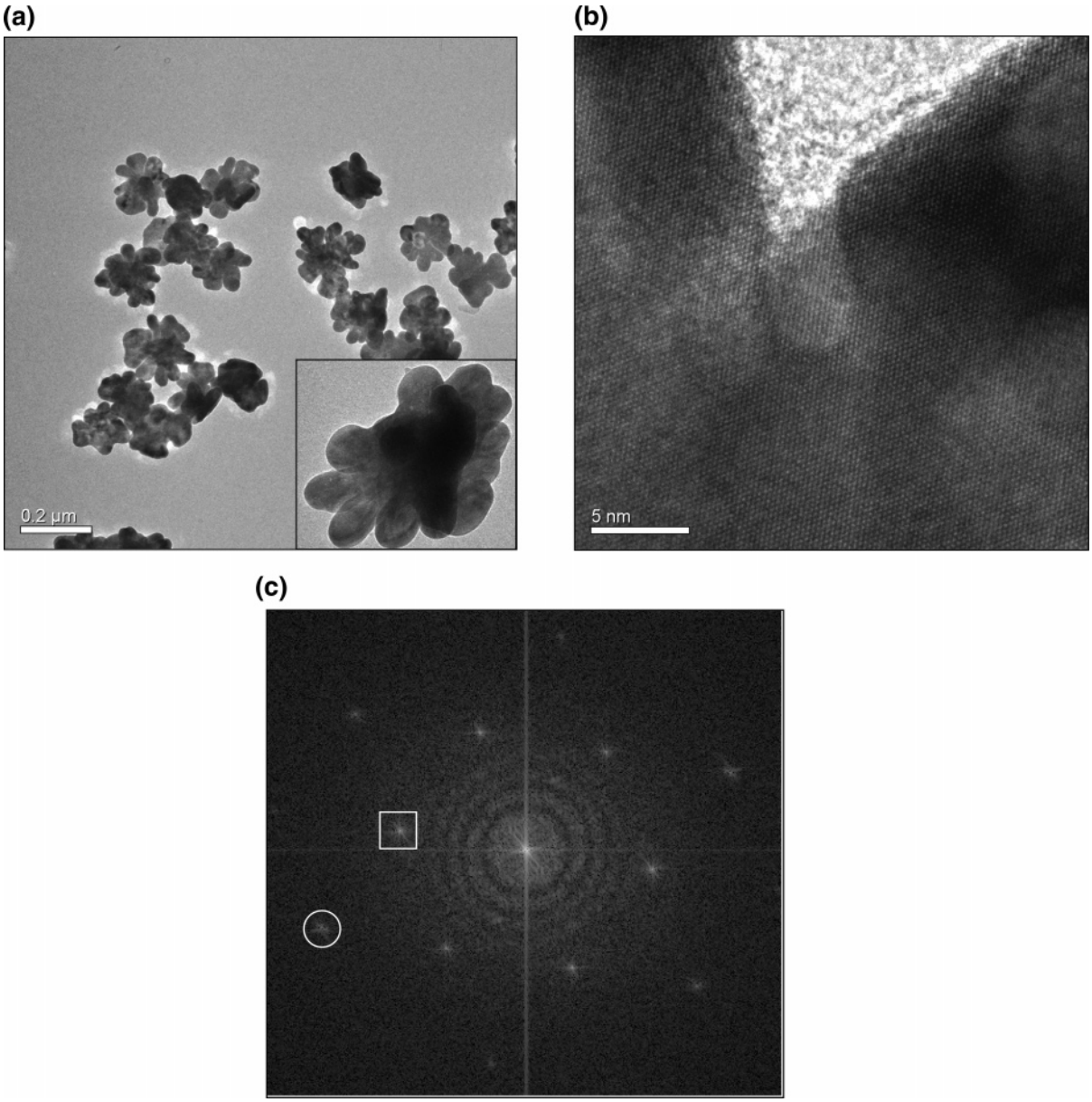

Figure 1. (a) TEM image of the flowerlike silver nanoplates (sample 1) and a corresponding higher-magnification image (inset), (b) HRTEM image of a conjuncting area between two "nanopetals" of the silver nanoplates, and (c) a corresponding FFT analysis.

38.12° in all the XRD patterns. This diffraction line is assigned to the (111) reflection for the fcc structure of metal silver with space group *Fm*3*m* (JCPDS, card no. 04-0783). However, diffraction lines corresponding to other crystal faces are sufficiently weak that they are barely discernible in the XRD patterns. This result clearly reveals that sample 1, sample 2, and sample 3 exclusively comprise the nanoplates that were preferentially oriented with their (111) planes parallel to the supporting substrate, thus giving a significantly high (111) reflection intensity, which further evidences our HRTEM observations.

Optical Properties of the Silver Nanoplates. The high anisotropy in shape of these nanoplates should substantially influence the resulting optical properties such as SPR and SERS, because the polarized moment is very much anisotropic.[7,8] Figure 4 shows UV−vis extinction spectra taken from the small silver seed and the products synthesized by changing the concentration of silver seed with other experimental conditions fixed. UV−vis extinction spectra of sample 1 and sample 2, shown in Figure 4a,b, respectively, exhibit three SPR bands. A shoulder band at around 340 nm is attributed to the out-of-plane quadrupole plasmon resonance of the silver nanoplates.[7] The second SPR band at the longest wavelength side (680 nm for sample 1, 624 nm for sample 2) is due to the in-plane dipole plasmon resonance,[7] which is very sensitive to the size and geometry of the products. It is noted that the in-pane dipolar resonance blue shifts with the increased concentration of silver seed. The third weak band located at 368 nm is probably due to the existence of a very small amount of spherical silver nanoparticles that are observed in TEM images. Similarly, the UV−vis extinction spectrum of sample 3 also shows the SPR bands at 340 and 585 nm, corresponding to out-of-plane quadrupole and in-plane dipole plasmon resonance of the silver nanoplates, respectively (Supporting Information, Figure S2c). Also, Figure 4c,d shows similar spectral characters, but an

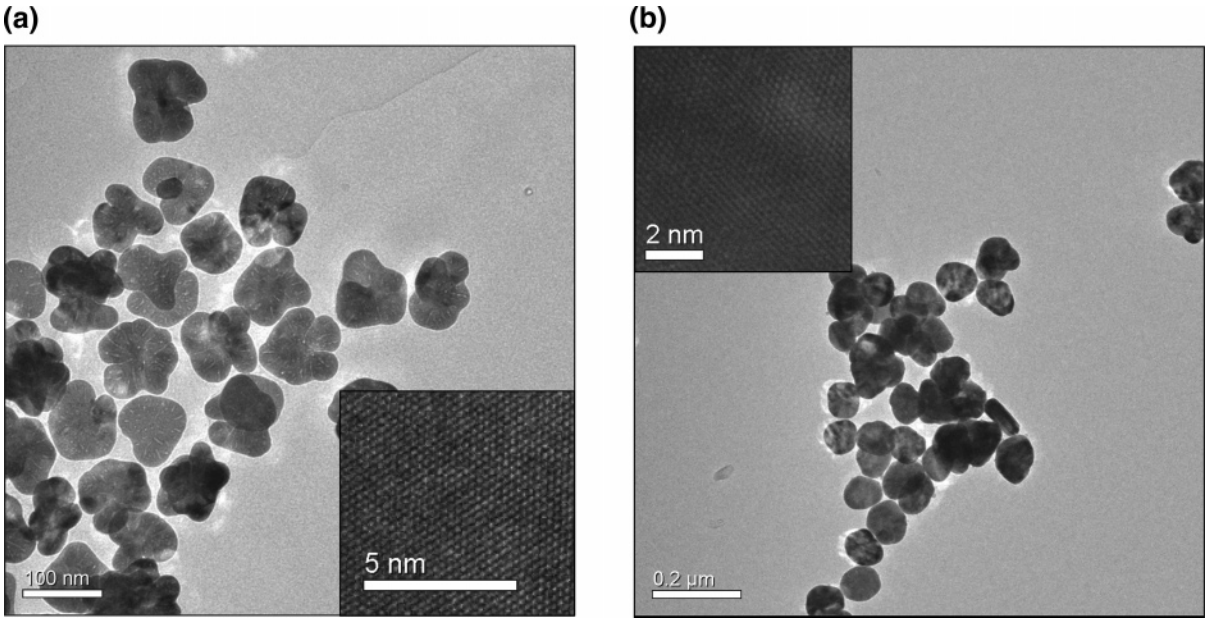

Figure 2. (a) TEM image of the flowerlike silver nanoplates (sample 2) and a corresponding HRTEM image (inset); (b) TEM image of the disklike silver nanoplates (sample 3) and a corresponding HRTEM image (inset).

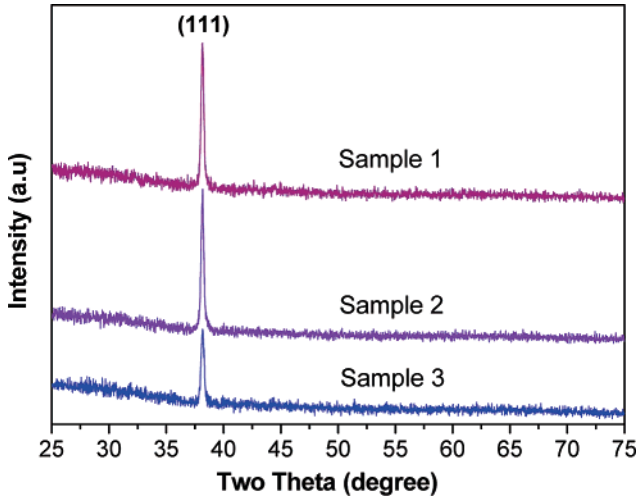

Figure 3. XRD patterns of three types of the silver nanoplates.

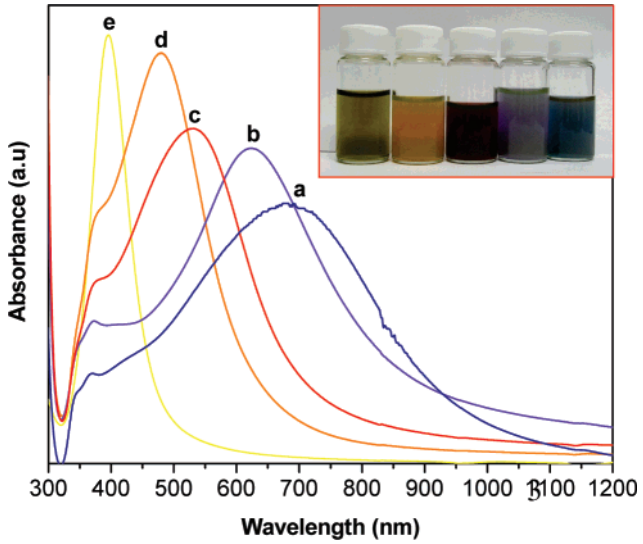

Figure 4. UV−vis extinction spectra of (a−d) the silver nanoplates synthesized in the presence of different amounts of the silver seed and 0.9 mL of 100 mM ascorbic acid: (a) 0.1 mL; (b) 0.2 mL; (c) 0.3 mL; (d) 1 mL, and (e) the silver seed. The inset shows the corresponding photographs (from right to left).

obvious blue-shift is observed relative to Figure 4a,b. The corresponding TEM images (Supporting Information, Figure S3) reveal their plate shapes and relatively smaller dimension. However, as indicated in Figure 4e, only one SPR band is observed at around 396 nm for the small silver seed. The inset in Figure 4 presents the photographs corresponding to Figure 4a−e, respectively (from right to left). It is evident that the color of the products varies from orange, to red, to purple, to blue, depending on the concentration of the silver seed.

We evaluated the performance of the three above-mentioned kinds of silver nanoplates for SERS application using R6G as a target molecule. For a comparison, spherical silver nanoparticles with an average diameter of 73 nm were prepared as a reference sample.[18] Figure 5a(1−4) compare the SERS spectra of the 10 nM R6G molecule obtained from sample 1, sample 2, and sample 3 and the spherical silver nanoparticles, respectively. A SERS spectrum characteristic of R6G is observed in each case, but clearly, two types of the flowerlike silver nanoplates exhibit the highest enhancement efficiency with the 514-nm excitation. Their SERS intensities of the peak at 1648 cm^{-1} are about 1 order of magnitude stronger than those from the spherical silver nanoparticles, while only about two-times intensity enhancement is observed for the disklike silver nanoplates. As stated in the Experimental Section, the above samples for SERS examination were prepared by drying the colloidal solutions on the glass substrates. This drying procedure can induce an aggregation of the silver nanostructures, which are highly desirable for surface Raman enhancement. Therefore, it is necessary to make it clear whether the high SERS ability of sample 1 and sample 2 depends on their special shapes. For

(18) Lee, P. C.; Meisel, D. *J. Phys. Chem.* **1982**, *86*, 3391.

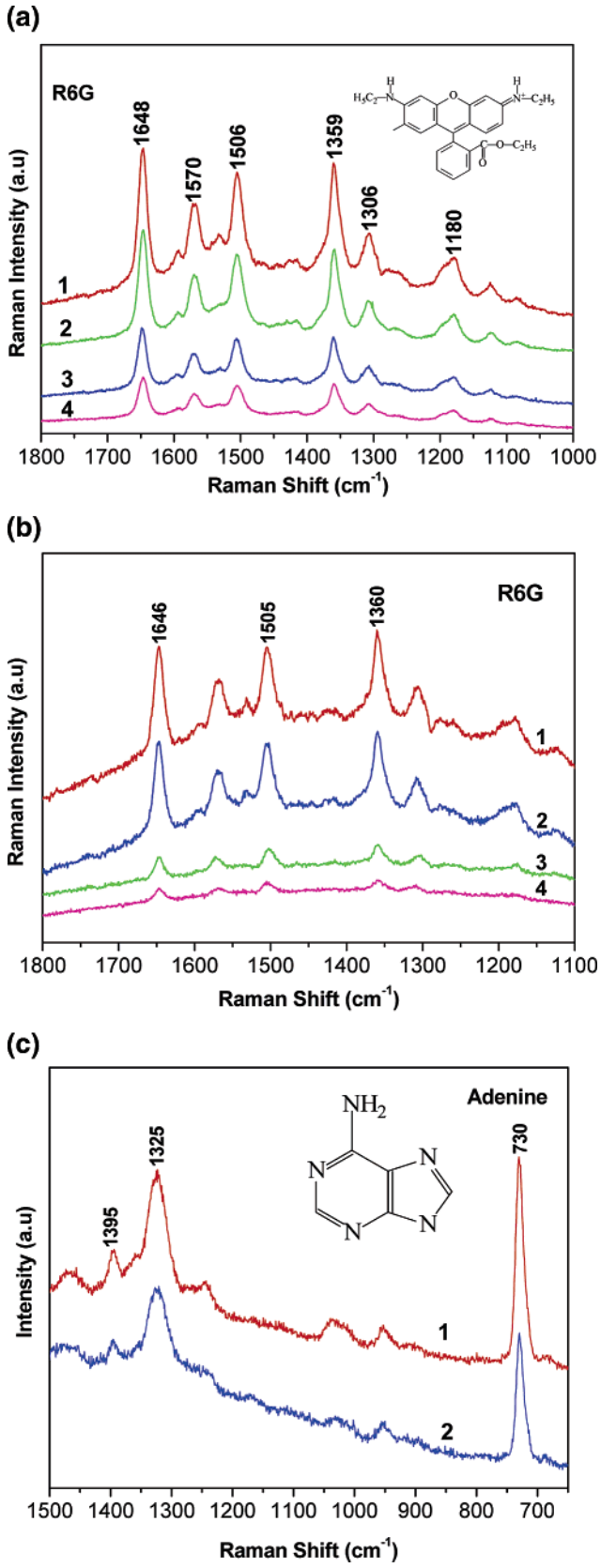

Figure 5. a: SERS spectra of 10 nM R6G molecules obtained from (1) sample 1, (2) sample 2, (3) sample 3, and (4) the 73-nm silver nanoparticles. The intensities of the spectra in (3) and (4) are multiplied by a factor of 3 for comparison purposes. b: SERS spectra of 50 nM R6G molecules collected from the colloidal solution of (1) sample 1, (2) sample 2, (3) the 73-nm silver nanoparticles, and (4) sample 3. c: SERS spectra of 1 μM adenine molecules on the surface of (1) sample 1 and (2) sample 2.

this purpose, we also investigate the SERS performance of the colloidal solutions of the above samples. The resulting SERS spectra of 50 nM R6G collected from the colloidal solutions of sample 1, sample 2, spherical silver nanoparticles, and sample 3 are shown in Figure 5b(1−4), respectively. As observed in Figure 5b, the colloidal solutions of the flowerlike silver nanoplates are also efficient for surface Raman enhancement, and the SERS signal intensity at 1648 cm^{-1} is about 5 times higher than that obtained from the colloidal solutions of the disklike silver nanoplates and the spherical silver nanoparticles. It is worth noting that the SERS signal intensities from the colloidal solution of the disklike silver nanoplates is weaker than that collected from the colloidal solution of silver nanospheres. These experimental results clearly reveal that the flowerlike nanostructures are a dominant contribution to large SERS signal enhancement of sample 1 and sample 2.

To explore the capability of the flowerlike silver nanoplates to detect nucleotide-based molecules, a DNA base adenine is also chosen as the target molecule. The SERS spectra of 1 μM adenine on sample 1 and sample 2, shown in Figure 5c(1−2), have two prominent Raman bands at 730 and 1325 cm^{-1}, corresponding to the purine ring breathing mode and the CN stretching mode, respectively.[19a] The SERS intensity of the peak at 730 cm^{-1} from sample 1 is about 1.6 times stronger than that from sample 2. The direct detection of nucleotide-based molecules including adenine is very important for rapid DNA sequencing where one method is based on spectroscopic detection and identification of single nucleotides.[19a]

The possible reasons for the larger Raman intensity enhancement on the flowerlike silver nanoplates can be considered as follows. SERS is a very local phenomenon occurring at crevices or in pores of the rough surface.[8a,19] In our case, the flowerlike silver nanoplates, as seen in Figure 1a, mainly consist of many interconnecting "nanopetals". Such structural features lead to the formation of many small crevices between the neighboring "nanopetals". Excited by the incident radiation, a collective surface plasmon is trapped between the neighboring "nanopetals", creating a huge local electric field at these crevices. For example, Xu et al. reported that an electric field enhancement of 10^{10} could be achieved between two nanoparticles with 1-nm spacing.[20] According to Pendry' calculations, these local resonant plasmon modes are able to produce the enhancement of as large as 10^7 in the Raman intensity of the target molecules adsorbed at these particular crevices.[21] Therefore, it is not surprising to observe that the flowerlike silver nanoplates exhibit higher Raman intensity enhancement than the disklike silver nanoplates and the spherical silver nanoparticles in our present experiment.

(19) (a) Kneipp, K.; Kneipp, H.; Itzkan, I.; Dasari, R. R.; Feld, M. S. *Chem. Rev.* **1999**, *99*, 2957. (b) Michaels, A. M.; Jiang, J.; Brus, L. *J. Phys. Chem. B* **2000**, *104*, 11965. (c) Wang, Z. J.; Pan, S. L.; Krauss, T. D.; Du, H. Rothberg, L. J. *Proc. Natl. Acad. Sci. U.S.A.* **2003**, *100*, 8638. (d) Schwartzberg, A. M.; Grant, C. D.; Wolcott, A.; Talley, C. E.; Huser, T. R.; Bogomolni, R.; Zhang, J. Z. *J. Phys. Chem. B* **2004**, *108*, 19191. (e) Jackson, J. B.; Halas, N. J. *Proc. Natl. Acad. Sci. U.S.A.* **2004**, *101*, 17930. (f) Hu, J. W.; Han, J. B.; Ren, B.; Sun, S. G.; Tian, Z. Q. *Langmuir* **2004**, *20*, 8831.
(20) Xu, H. X.; Bjerneld, E. J.; Käll, M.; Börjesson, L. *Phys. Rev. Lett.* **1999**, *83*, 4357.
(21) Garcia-Vidal, F. J.; Pendry, J. B. *Phys. Rev. Lett.* **1996**, *77*, 1163.

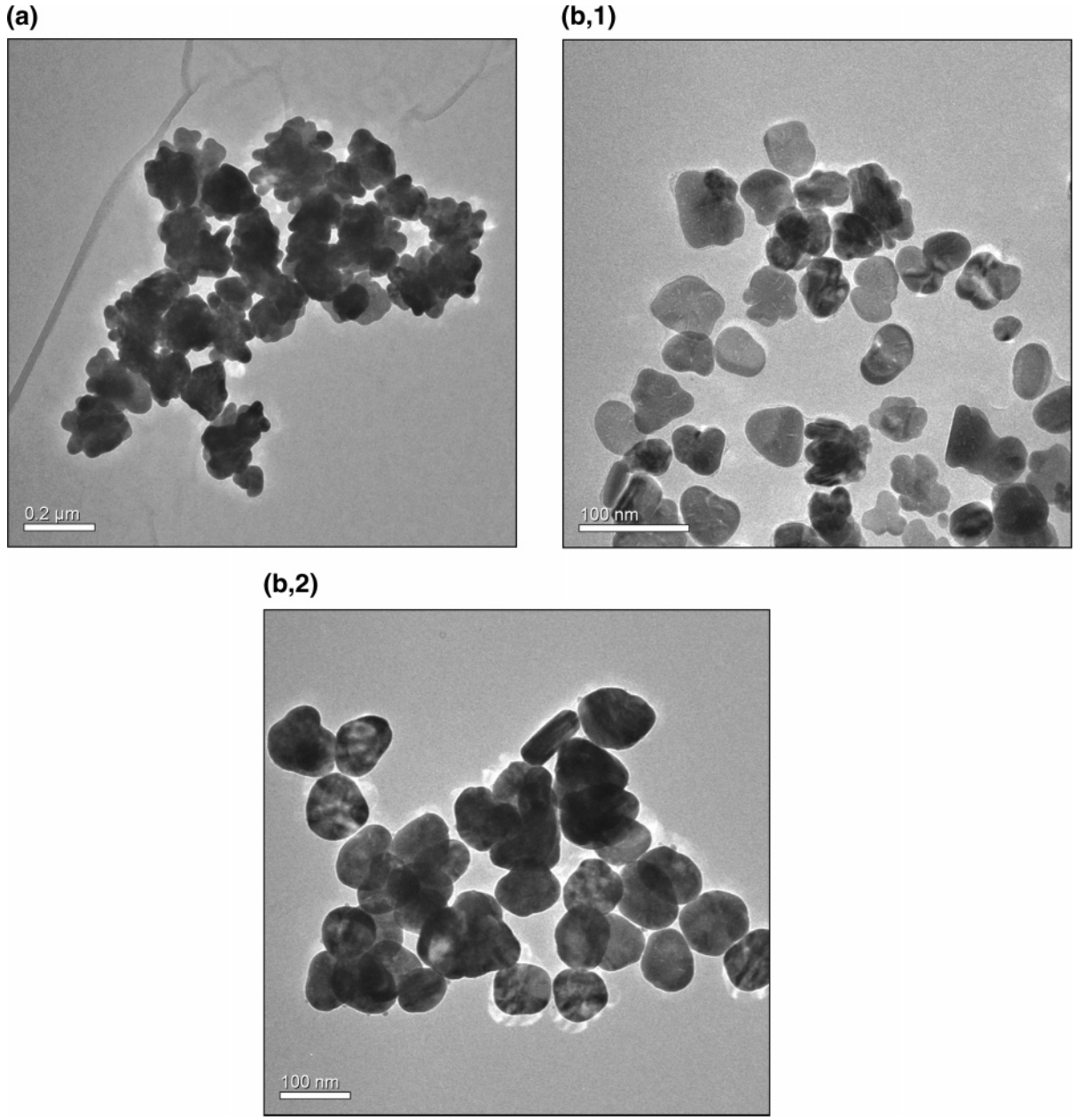

Figure 6. a: TEM image of the silver nanoplates synthesized with the PVP/$Ag(NH_3)_2^+$ molar ratio of 0.4. b: TEM images of (1) the silver nanoplates prepared with 80 μL of 100 mM ascorbic acid and in the absence of silver seed and (2) the silver nanoplates prepared with 80 μL of 100 mM ascorbic acid and 300 μL of silver seed.

Possible Formation Mechanism. To gain control of the synthesis, it is necessary to understand the mechanism by which the silver nanoplates with special shapes are formed. Like most fcc metals, metal silver has a cuboctahedral equilibrium shape dominated by the {111} faces and the {100} faces because these faces have the lowest energies.[22] A general order of the surface energies for different faces of the fcc metals may hold, $\gamma_{\{111\}} < \gamma_{\{100\}} < \gamma_{\{110\}}$.[23] That is, more energy is released by adding a silver atom to the {100} faces or the {110} faces other than the {111} faces during crystal growth. As a result, crystal growth can be accelerated by biasing accretion onto a {100} face, a {110} face, or others, thus increasing the area of the {111} faces.[24] It is generally accepted that the shape of fcc metal nanostructures is mainly determined by the growth rate along the ⟨100⟩ versus the ⟨111⟩ orientation.[23] In our case, both the flowerlike and the disklike silver nanoplates possess one large {111} basal face. Accordingly, it is reasonable to conclude that the as-prepared silver nanoplates must be nonequilibrium ones and their shapes must be mediated by a process that prevents addition of silver atoms to the {111} faces as rapidly as to other faces. This can occur either by slowing the growth rate along the ⟨111⟩ orientation or by increasing the growth rate, such as along the ⟨100⟩ and the ⟨110⟩ orientation.

As stated above, the success of the proposed method strongly relies on the proper choice of the precursors including $Ag(NH_3)^+$ and ascorbic acid, through which the

(22) (a) Cleveland, C. L.; Landman, U. *J. Chem. Phys.* **1991**, *94*, 7376. (b) Brown, S.; Sarikaya, M.; Johnson, E. *J. Mol. Biol.* **2000**, *299*, 725.
(23) Wang, Z. L. *J. Phys. Chem. B* **2000**, *104*, 1153.
(24) Porter, D. A.; Easterling, K. E. *Phase Transformations in Metals and Alloys*; Chapman and Hall: London, 1992.

reduction process of silver salts proceeded in a mild way. Furthermore, we investigated the effect of PVP, the silver seed, ascorbic acid, and sodium citrate concentration on the formation of these silver nanoplates with special shapes. In the synthesis of sample 1, the molar ratio between PVP and $Ag(NH_3)^+$ is about 1.2. When we decreased this molar ratio to 0.42, while keeping other experimental conditions fixed, the flowerlike silver nanoplates were also observed, but an obvious aggregation occurred for them (Figure 6a), suggesting that the primary role of PVP in this process is to stabilize the silver nanoplates with good monodispersity. However, if the reduction reaction of $Ag(NH_3)^+$ by ascorbic acid was performed in the absence of sodium citrate, the spherical silver nanoparticles were the dominant products. This result shows that sodium citrate plays an important role in the shape control of the silver nanoplates. Other groups also reported that citrate ions were critical for the formation of highly anisotropic metal nanostructures.[7a,b,12e,25,26] As mentioned above, the shape of the as-prepared silver nanoplates is dependent upon the concentrations of silver seed and ascorbic acid. The presence of small silver seed as nucleation sites can catalyze the reduction processes of $Ag(NH_3)^+$ by ascorbic acid due to particle-mediated electron transfer from ascorbic acid to the $Ag(NH_3)^+$ ions. As inferred from the color change of the reaction solution, the fewer the initial nucleation sites, the slower the reduction rate of the $Ag(NH_3)^+$. Both the disklike and the flowerlike silver nanoplates were found to form only at the low concentration of silver seed. This dependence implies that the slow reduction rate is favorable for the formation of highly anisotropic silver nanoplates. Interestingly, it was noted that, in the absence of silver seed, the silver nanoplates with shapes of disk and flower could also be produced at a low concentration of ascorbic acid, probably because the low concentration of ascorbic acid led to the decrease in the number of nucleation sites in the reaction solution (Figure 6b1). Nevertheless, the quality of the resultant silver nanoplates are poor relative to that in the presence of the silver seed (Figure 6b2), indicating that the proper combination of silver seed and ascorbic acid is necessary for synthesizing the good-quality silver nanoplates with special shapes. Their three-dimensional shapes were also verified by tilting the sample plane (Supporting Information, Figure S4). On the basis of the evidence discussed so far, we suggest the silver nanoplates with shapes of disk and flower are formed as follows. In the presence of the single-crystal silver seed, which was preformed or obtained by direct reduction, selective adsorption of citrate ions on the {111} faces of the silver seed resulted in the preferential addition of silver atoms to the other crystal faces such as the {110} faces. Accordingly, such selective interaction slowed the growth rate along the ⟨111⟩ direction and thus promoted a highly anisotropic growth in other directions such as the ⟨100⟩ and ⟨110⟩ directions, extending into large nanoplates with the {111} basal faces and ultimately leading to selective growth of the silver nanoplates with different shapes.[22,23] Furthermore, because the adsorption of citrate ions on other faces was weak, oriented growth could be controlled through changing the concentration of silver seed and ascorbic acid, which is the reason the concentrations of silver seed and ascorbic acid have important effects on the shape control of the silver nanoplates.[16]

In summary, we have demonstrated a new strategy for the high-yield, controlled synthesis of the silver nanoplates with shapes of disk and flower. The shape control of the silver nanoplates provides an interesting way to tune their optical properties. Thanks to their high anisotropy in shape, the novel flowerlike silver nanoplates exhibit excellent SERS enhancement ability relative to the spherical silver nanoparticles and the disklike silver nanoplates, which are expected to have wide applications in biosensors and other related fields. Further modification of our methods can create many other types of the metal nanostructures with unusual shapes.

Acknowledgment. The authors would like to thank Youhei Ando for XRD measurement and Shin Watanabe for SEM examination. This work was partially supported by "Open Research Center" project for private universities: matching fund subsidy from MEXT (Ministry of Education, Culture, Sports, Science and Technology), 2001−2008.

Supporting Information Available: SEM, TEM, UV−vis data, and calculation of interplanar angle (PDF). This material is available free of charge via the Internet at http://pubs.acs.org.

CM0615875

(25) Sun, Y. G.; Xia, Y. N. *Adv. Mater*. **2003**, *15*, 695.
(26) Callegari, A.; Tonti, D.; Chergui, M. *Nano Lett.* **2003**, *3*, 1565.